

Seismic record of a long duration dispersive signal after the 15 January 2022 Hunga-Tonga eruption

J. Diaz  *1

¹Geosciences Barcelona (GEO3BCN), CSIC, Barcelona, Spain

Author contributions: *Conceptualization, Funding Acquisition, Investigation, Methodology, Validation, Visualization, Writing – original draft, Writing – review & editing:* J. Diaz.

Abstract Data acquired by broadband seismic stations distributed around the world are used to document the exceptionally long duration signal from the tsunami-associated gravity wave that followed the January 2022 Hunga-Tonga eruption. The first arrivals of this wave, with a frequency of around 2 mHz, are recorded at the time the tsunami arrives to each station, but the highest recorded frequencies, which reach 40 mHz, arrive 5 days later at some sites, following the prediction of a gravity wave originating at the Hunga-Tonga region and traveling in deep water. This dispersive signal is detected in most of the stations located in the Pacific Ocean basin and its coasts, but also in the Indian Ocean, Antarctica, and some stations in North America located hundreds of kilometers from the coastline. The signal is compared with the data gathered after earthquakes that have produced large tsunamis, showing that the seismic records from the Hunga-Tonga eruption are very different. Following the hypothesis pointed out by Omira et al 2023, we propose that the origin of this exceptional characteristic is due to the interaction between the tsunami and atmospheric waves that travel a little faster.

Production Editor:
Gareth Funning
Handling Editor:
Lise Retailleau
Copy & Layout Editor:
Hannah F. Mark

Signed reviewer(s):
Brad Lipovsky

Received:
June 28, 2023
Accepted:
October 26, 2023
Published:
November 29, 2023

1 Introduction

On January 15 2022, the Hunga-Tonga (H-T) volcano, located in the South Pacific Ocean, produced one of the most powerful volcanic events recorded to date, with an estimated TNT equivalent yield of 100-200 Mt (Vergoz et al., 2022) and a plume that reached 55 km high (Carr et al., 2022). This exceptional eruption generated a large seismic earthquake and powerful atmospheric waves, detected by multiple instruments throughout the world, from simple weather stations to satellites, infrasound detectors, microbarographs, tidal gauges, geodetic stations, and broad-band seismic stations. The effects of the violent eruption reached even the ionosphere, where they produced significant variations in the ionospheric total electron content (TEC) (e.g. Astafyeva et al., 2022). Probably the most outstanding feature after the H-T eruption was the atmospheric wave generated by the eruption, characterized by a sudden variation in pressure. The wave's passage was recorded during at least four laps of the planet. Various publications have shown that most of the energy injected into the atmosphere propagated as a Lamb wave (e.g. Amores et al., 2022). Atmospheric Lamb waves are characterized by their low-frequency range, typically below 10 mHz, their non-dispersive character, and their ability to travel long distances without significant attenuation. Analysis of the Lamb waves generated by the H-T eruption has shown that their propagation velocity is close to 310 ms⁻¹ and that the pressure variations have been in the range of hundreds of Pascals (Matoza et al.,

2022). Wright et al. (2022), based on the analysis of satellite images for several hours, also identified the propagation of gravity waves in the atmosphere, travelling with phase speeds between 240 and 270 ms⁻¹ and showing frequency dispersion. As these authors pointed out, gravity waves that remain coherent and spread across the globe are unprecedented.

The H-T eruption generated an exceptional tsunami, recorded on a global scale, with a very long duration and unexpected wave heights in the far field (e.g. Omira et al., 2022). The onset of this tsunami was detected earlier than expected by tsunami propagation models, as the direct tsunami was preceded by a distinct, fast-travelling, moderate height tsunami that was clearly detected worldwide, arriving several hours before the main one (e.g. Carvajal et al., 2022; Zhou et al., 2023; Ho et al., 2023). This kind of feature, interpreted to result from the large pressure oscillation generated by the Lamb wave passing over the location, was first described by Harkrider and Press (1967) after the Krakatoa eruption and it is often called a meteotsunami (e.g. Denamiel et al., 2023). The main tsunami waves were observed on coastal tide gauges distributed throughout the world, although the largest values, with heights >3 m, were recorded off the coasts of California and Chile (Carvajal et al., 2022). The arrival time of these waves agrees well with the theoretical travel times of a free tsunami wave originating in the vicinity of the volcano at the time of the eruption and traveling at 198 ms⁻¹, the speed corresponding to the average depths of the Pacific waters. As shown by Ho et al. (2023), the differences in time and amplitude of both surges are af-

*Corresponding author: jdiaz@geo3bcn.csic.es

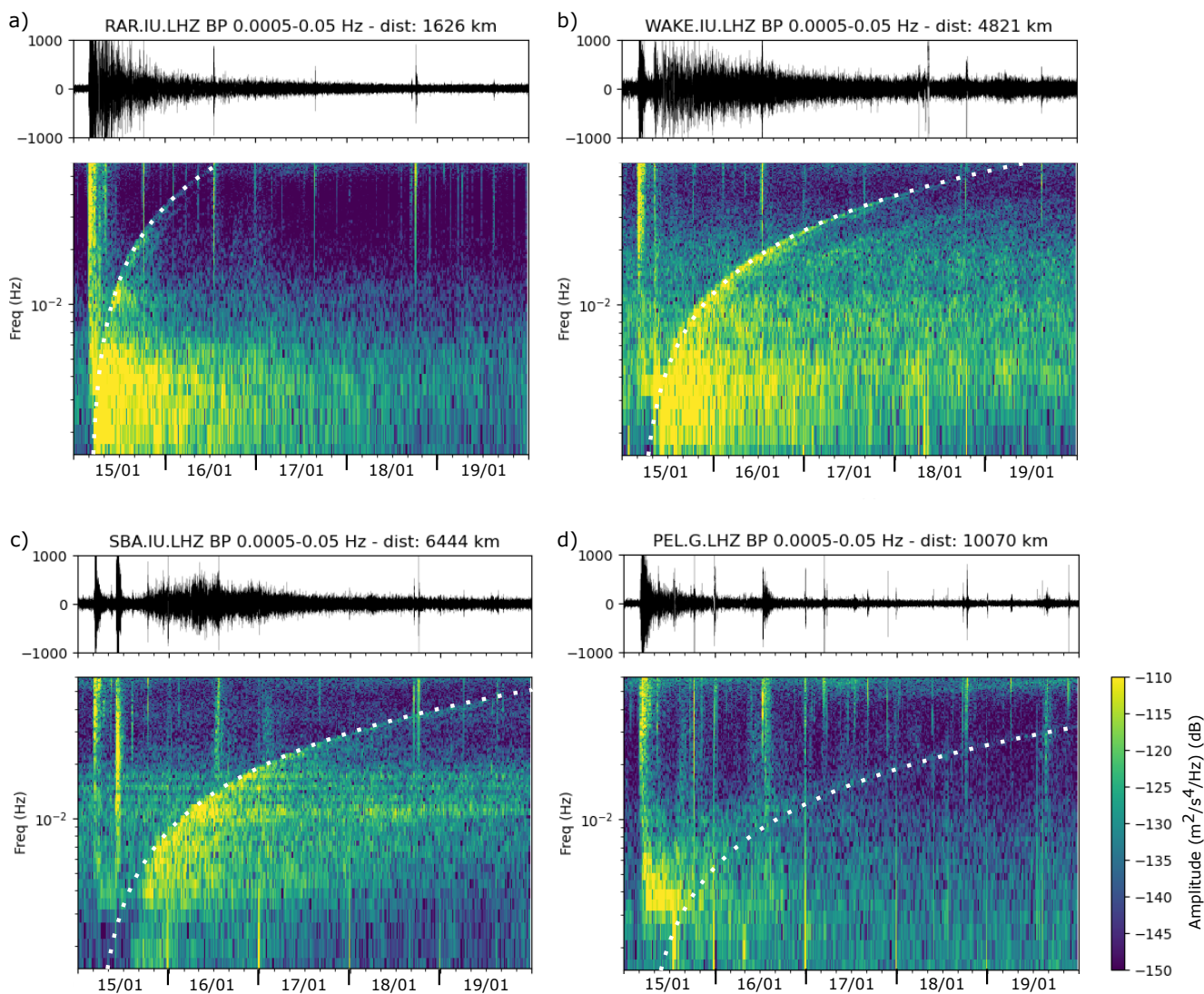


Figure 1 Examples of the long-duration dispersive arrivals detected at stations on the Pacific islands of Rarotonga (RAR) and Wake (WAKE), Antarctica (SBA), and Central Chile (PEL). Frequency is represented using a logarithmic scale. White dashed lines show the gravity dispersion curves.

ected by the bathymetry variations along their path. Zhou et al. (2023) noticed that the pressure disturbances produced by the Lamb wave (<200 Pa) are not sufficient to explain the relatively large amplitudes of the meteo-tsunami waves observed in some areas, particularly near the coast of Japan. They analyzed if this amplification could be related to the Proudman resonance, and concluded that it is better explained by nearshore amplification effects. However, Lynett et al. (2022) suggested that the air-pressure passing over the deep-water subduction zones in the Pacific triggered a Proudman resonance effect, with each major trench in the Pacific Basin generating a small tsunami. These multiple tsunamis could explain the persistent sea-level perturbations in the Pacific coasts.

The main phase of the eruptive process included four large explosions, observed in satellite data and generating seismic waves detected around the world. The main explosion, at 04:14 on January 15, 2022, was detected by global seismic networks, which assigned a magnitude of 5.8 to the event. This explosion resulted in the ex-

citation of Earth normal modes, with the planet pulsing every 4.5 minutes for more than 4 hours (Diaz, 2022; Garza-Girón et al., 2023; Ringler et al., 2022). Broadband seismometers also recorded the successive passages of the Lamb waves, showing that the associated pressure variations were, even after traveling four times around the planet, strong enough to be detected in an instrument not specifically designed to detect them (Diaz, 2022).

In this contribution, seismic data recorded around the world are used to document another of the features that make post-eruption seismic records exceptional: the recording of surface gravity waves (SGW), in a frequency range between 5 and 50 mHz, which can be identified continuously in some places for time intervals up to five days. Although long-lived, dispersive SGW generated by cyclones have been reported in seismic data recorded on the Antarctic ice shelves (e.g. Cathles et al., 2009), there are no previous examples to my knowledge of any signal being recorded continuously for such a long time interval all around the world. I show some

representative examples of the signal, compare the seismic records with hydroacoustic and deep-water pressure sensor data, analyze the differences between the seismic signal of the tsunami generated by the H-T eruption and the seismic records of large tsunamis, comment on the global distribution of the observations, and finally discuss the possible origins of this signal.

2 Seismic observations of tsunami-related dispersive signals

Data from low sampling channels from broadband seismic stations distributed all over the globe and integrated into the main worldwide large-scale seismic networks, including the Global Seismograph Network (Albuquerque Seismological Laboratory/USGS, 2014), IRIS/IDA seismic network (Scripps Institution of Oceanography, 1986), Geoscope (IPGP and EOST, 1982), and Geofon (GEOFON Data Centre, 1993), were retrieved, using the IRIS online services, to investigate the seismic record of the H-T tsunami. Data were merged into files of seven days of duration, from January 15 to 21, 2022, and transformed to the frequency-time domain using Obspy routines based on the classical FFT transform (Megies et al., 2011; Krischer et al., 2015). Spectrograms were calculated using a window length of 1800 s, with 80% overlap.

As stated above, I will focus on the long-duration dispersive signal that dominates the spectrograms in the 5-50 mHz band for time intervals ranging from one to five days. Fig. 1 shows the records of this signal at four representative stations located on Rarotonga and Wake Islands in the Pacific Ocean, Scott Base in Antarctica, and central Chile, covering distances between 1600 and 10000 km from H-T. The strong dispersive character of this feature, the wave onset propagation time, and the variable slope of the signal show that its origin is the main tsunami wave generated by the H-T eruption propagating across the ocean. To confirm this point, I have calculated the dispersion curves of a gravity wave assuming propagation in deep water. In this case,

$$v_p = \sqrt{\frac{g}{k}} = \frac{d}{t} \quad (1)$$

and

$$v_g = \frac{1}{2} \sqrt{\frac{g}{k}} \quad (2)$$

where g is gravity, k is the wavenumber, d is distance, t is propagation time, and v_g and v_p are group and phase velocities, respectively. Then,

$$k = \frac{g}{v_p^2} = \frac{g}{(2v_g)^2} = \frac{gt^2}{4d^2} \quad (3)$$

and, from the classical equation

$$\omega = \sqrt{gk} = 2\pi f \quad (4)$$

we can estimate frequency as a function of time for any given distance. White dashed lines in Fig. 1 show the resulting curves for each distance range, proving that this is the origin of the signal. The mismatches observed at

the lower frequencies for distant sites can be explained by the deep water hypothesis, and do not affect to the interpretation of the signal. The identification of the first arrival of the dispersive curve is difficult since, on the one hand, the high energy Lamb wave, with frequencies below 5 mHz, arrives relatively close and, on the other hand, the excitation of the normal nodes on Earth generate a relatively large energy at 0.3 mHz for hours after the eruption (e.g. Diaz, 2022; Ringler et al., 2022).

The dispersive character of oceanic surface gravity waves (SGW) was first observed in the late 1950s by Munk and Snodgrass (1957), who analyzed the incoming swell at Guadalupe Island (Mexico) and showed that the wave trains had an increasing frequency. Broadband seismometers deployed on Antarctic ice shelves have provided multiple examples of days-long SGW generated by storms, as shown by Cathles et al. (2009), MacAyeal et al. (2006) or Lipovsky (2018). Recently, Hell et al. (2019) have proposed a method to use these data to verify the position of high wind speed areas over the Southern Ocean and Aster et al. (2021) have shown that the swell interaction with the Ross Ice shelf triggers small, near-front seismic signals.

SGW related to the Hunga-Tonga eruption have been observed by Le Bras et al. (2022) in the data recorded by four of the hydroacoustic sensors deployed in shallow waters by the International Monitoring System (IMS) network in the Pacific Ocean. In order to compare with the seismic records and confirm the common origin of the signals, I have recovered the data from the H11S1 instrument, located close to Wake Island, where seismic data is available. Additionally, I have recovered the data from the microbarometric sensor WAKE.IU.LDO, co-located with the seismic instrumentation. The spectrograms of the three sensors, shown at Fig. 2, have been calculated using the same parametrization in all the cases but are represented using adapted amplitude scales to better highlight the amplitude variations. As observed, the microbarograph (Fig. 2a) clearly records the passage of the Lamb waves traveling in opposite directions of the great arc (red and orange arrows) and no evidence of a tsunami-related signal is detected. The broad-band seismic data (Fig. 2b) is dominated in this frequency range by the tsunami-related dispersive wave. The arrival of the seismic waves, a few minutes after the H-T explosion, is observed at frequencies higher than 10 mHz. The first passage of the Lamb wave is detected as a low frequency signal preceding the arrival of the oceanic tsunami signal. For frequencies above 20 mHz, several teleseismic events can be identified, the most prominent corresponding to a M 6.1 earthquake with epicenter in Papua-Guinea on 16 January around 13:00.

The in-water hydroacoustic sensor (Fig. 2c) shows the dispersive gravity wave associated with the tsunami, visible between 8 and 50 mHz and clearly consistent with the seismic data. Le Bras et al. (2022) noted the presence of a secondary dispersive signal at this station, interpreted as an effect of the tsunami propagation through the Tonga-Kermadec trench. This signal is also clearly observed in the seismic data, which seems to provide the most complete record of the event at this location.

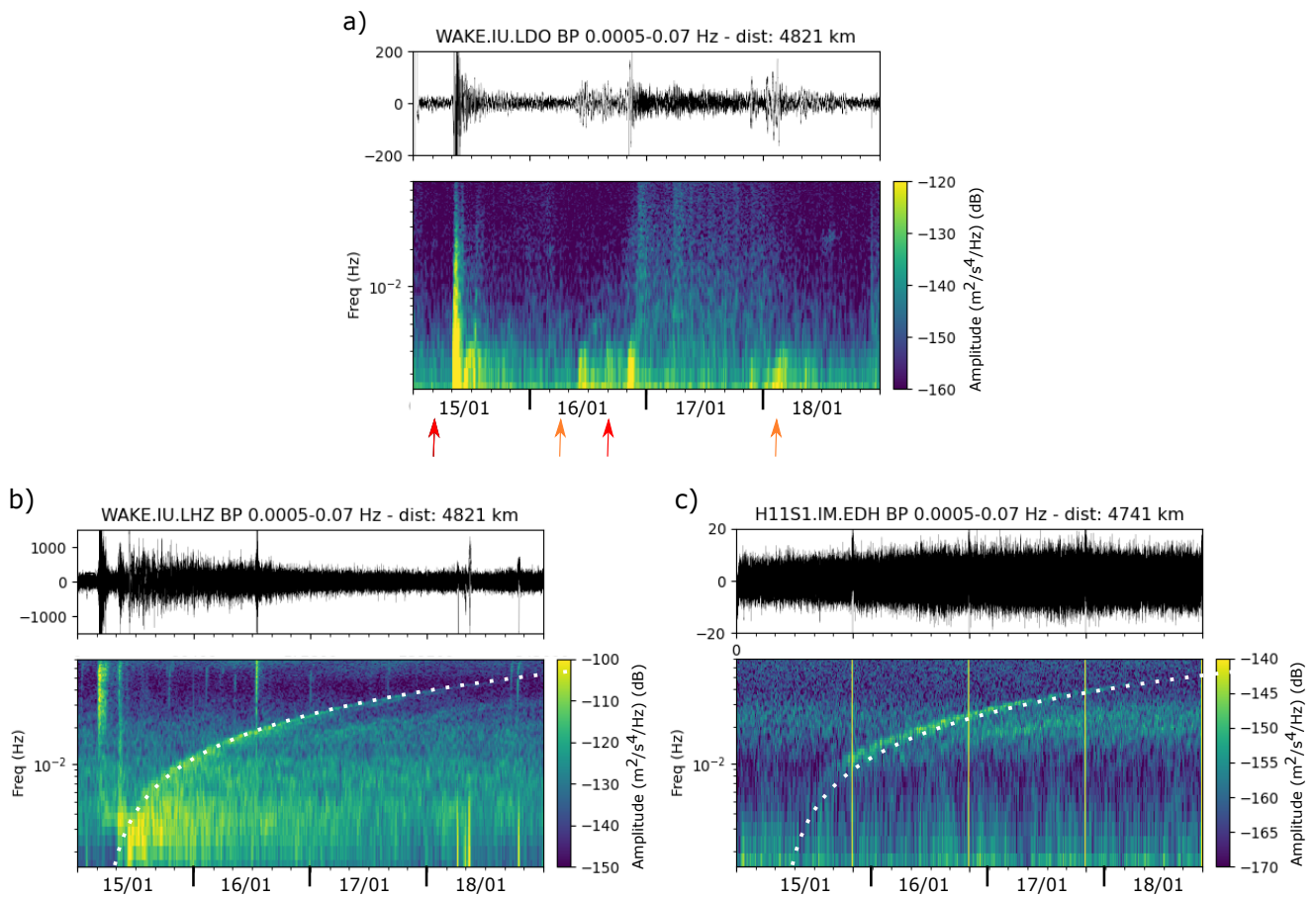


Figure 2 Waveforms and spectrograms for the microbarograph (a), broad-band station (b), and hydroacoustic sensor (c), located at Wake Island (North Pacific). The upper panels show the corresponding waveform, filtered between 0.5 and 70 mHz. The red and orange arrows in (a) show the arrival of Lamb waves. Dotted lines in (b) and (c) show the gravity wave arrival.

3 Uniqueness of the observation

The recording of tsunamis on near-shore seismic stations has been described previously (e.g., Yuan et al., 2005; Okal, 2007; Poplavskiy and Le Bras, 2013). However, the seismic recording of the oceanic gravity wave presented so far is limited to a few hours of duration following the tsunami arrival. There are not, to my knowledge, previous reports of dispersion curves related to oceanic gravity waves being recorded during several days by broad-band seismometers. To check the uniqueness of the event, I have recovered the seismic data recorded during the 5 days following the Chile 2010 M8.8, Tohoku 2011 M9.1, and Sumatra 2004 earthquakes, that resulted in three of the largest tsunamis recorded in the Pacific. Fig. 3 shows the spectrograms of the H-T event compared to those for these large earthquakes for stations located at Rarotonga (Cook Islands), Wake Island, and Eastern Island, all of them in the Pacific Ocean.

As noted, for large earthquakes the spectrograms in the 0.5-70 mHz range are dominated by arrival of the surface waves that circle the Earth every 3.5 hours, showing a decay on their frequency content. The amplitude of the waveform is two orders of magnitude larger for the earthquakes than for the H-T eruption, indicating that the seismic energy generated by H-T main erup-

tive episode was not exceptional. However, the long-lived dispersive oceanic gravity wave can only be identified for the H-T eruption, hence suggesting that this signal is not only related to the energy associated with the tsunami, but is probably boosted by a secondary mechanism.

4 Geographical distribution of the tsunami-related seismic signals

As commented above, I have retrieved the data for the vertical components of seismic stations of the global scale networks that distribute low sampling channels (LHZ, 1 sample per second). Data has been recovered for 134 locations covering Australia, Africa, the Americas, Europe, and a large number of islands in the Pacific and Indian oceans. The tsunami-associated gravity wave has been identified in 46 of these sites, 34% of the inspected sites, at distances ranging from 750 to 12500 km from H-T. Supplementary Figure S1 shows the waveforms and spectrograms of the stations with positive identifications of the signal, ordered accordingly to their distance.

As observed in Fig. 4, this feature has been identified for most of the stations located on islands in the Pacific basin and near the coasts surrounding this ocean

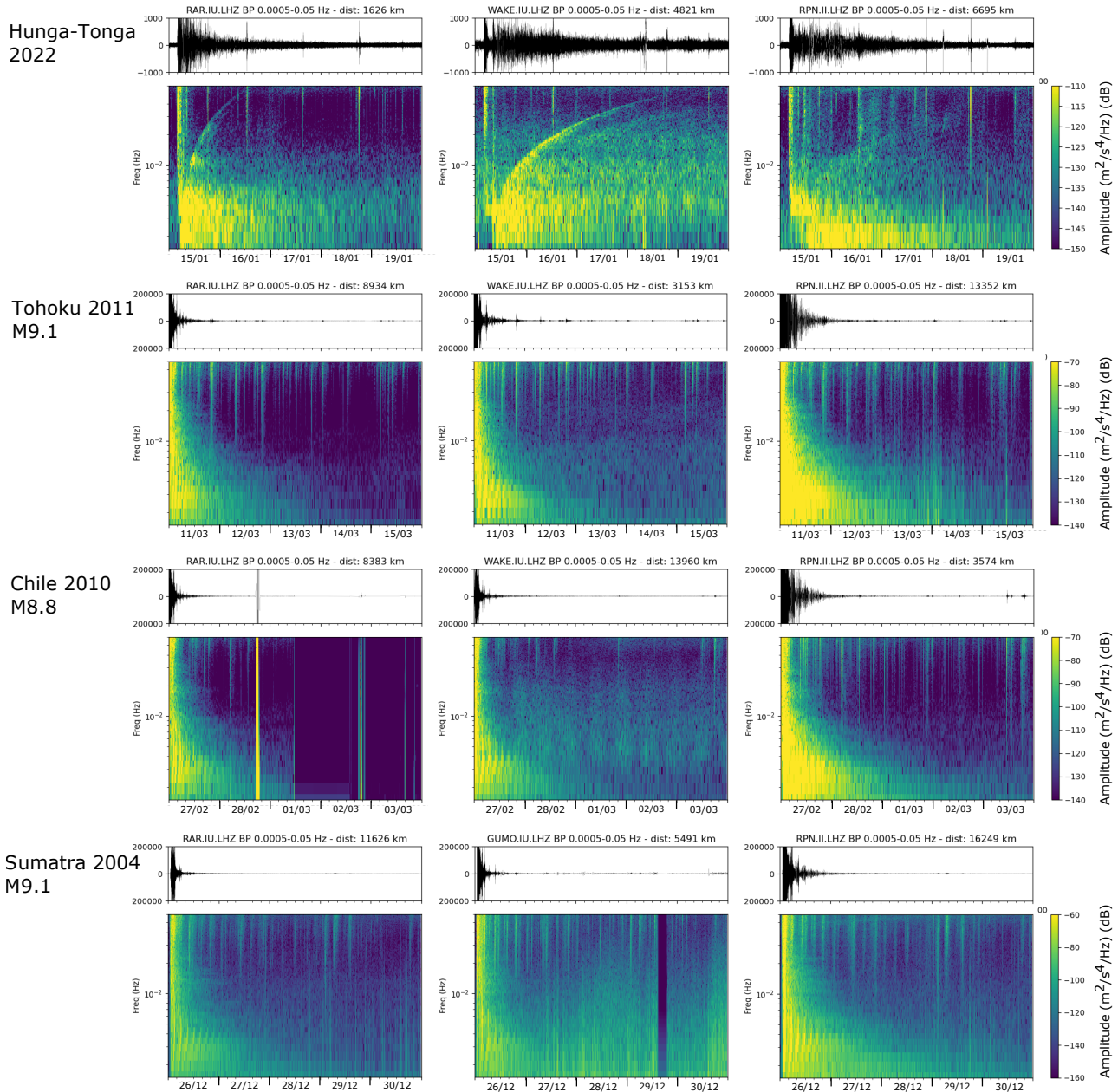


Figure 3 5-day long spectrograms after the H-T eruption at 3 sites in the Pacific Ocean, compared to records at the same sites after the Tohoku 2011 M9.1, Chile 2010 M8.8, and Sumatra 2004 M9.1 earthquakes. For the Sumatra event, WAKE records are not available and GUMO station is used instead.

(Japan, New Zealand, North, Central, and South America). Although some energy around 10 mHz is observed at times consistent with the gravity wave arrival, the two stations located on the Hawai’ian islands (KIP and POHA) show no evidence of the signal, suggesting that local conditions play a role in its detection. Fig. 5 shows the waveforms and the spectrograms at sites along a transect oriented approximately E-W across the SE Pacific Ocean (Rarotonga, Pitcairn and Eastern Islands), crossing the southern part of the Andes and reaching the Atlantic ocean at the South Georgia Islands. Although it is difficult to identify the tsunami-related signal in the filtered waveforms, the spectrograms clearly evidence the signal, which can be identified for several

days at the most distant sites and is restricted to frequencies below 50 mHz. The figure also proves that the dispersive signal is not a local effect, but originates from the H-T eruption.

Many sites located along the Pacific coasts of North, Central, and South America detect the signal for intervals of two to four days after the first arrival, despite being located far from the coasts (Fig. 6a). It should be noted that the largest water heights reported by coastal tidal gauges correspond to sensors located in Chile and western North America (Carvajal et al., 2022). More surprisingly, stations located within the North American continent, in places like Tucson (Arizona), Albuquerque (New Mexico), and South Dakota show a low-energy dis-

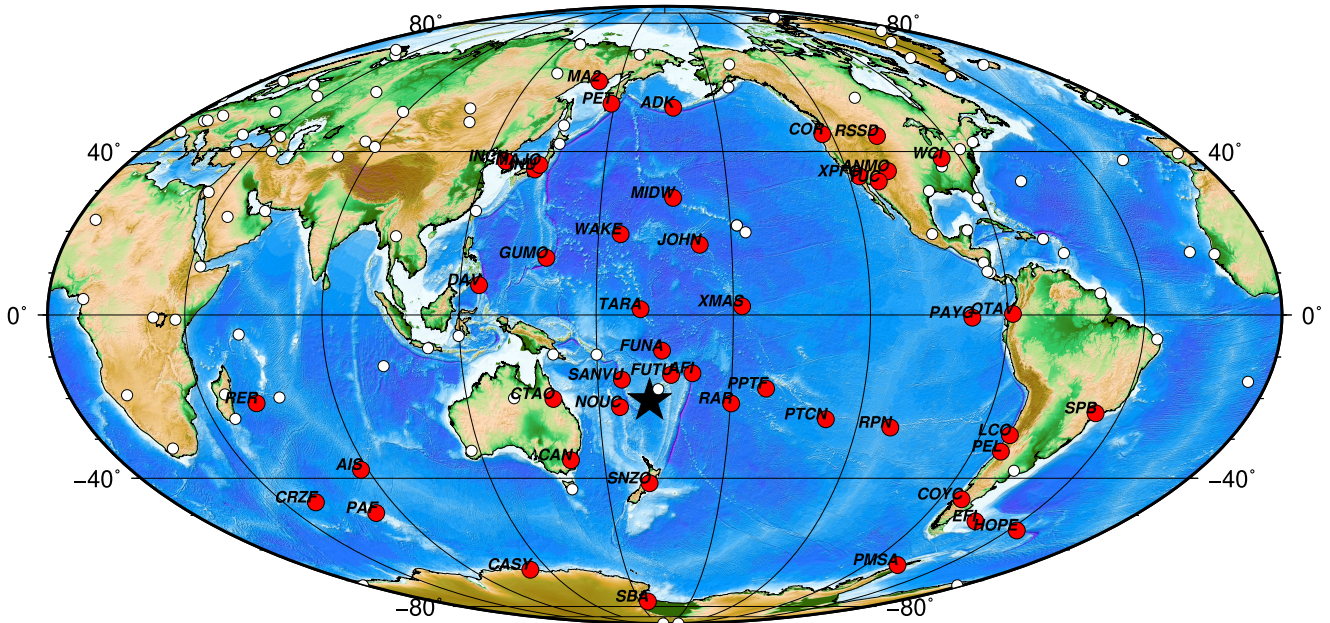


Figure 4 Map showing the locations where the tsunami-related dispersive signal has been identified (red dots). The black star shows the location of the H-T volcano and the white dots show the seismic stations where this signal has not been identified. Topography and bathymetry are from the ETOPO2 Gridded Globe Relief Data (National Geophysical Data Center, 2006).

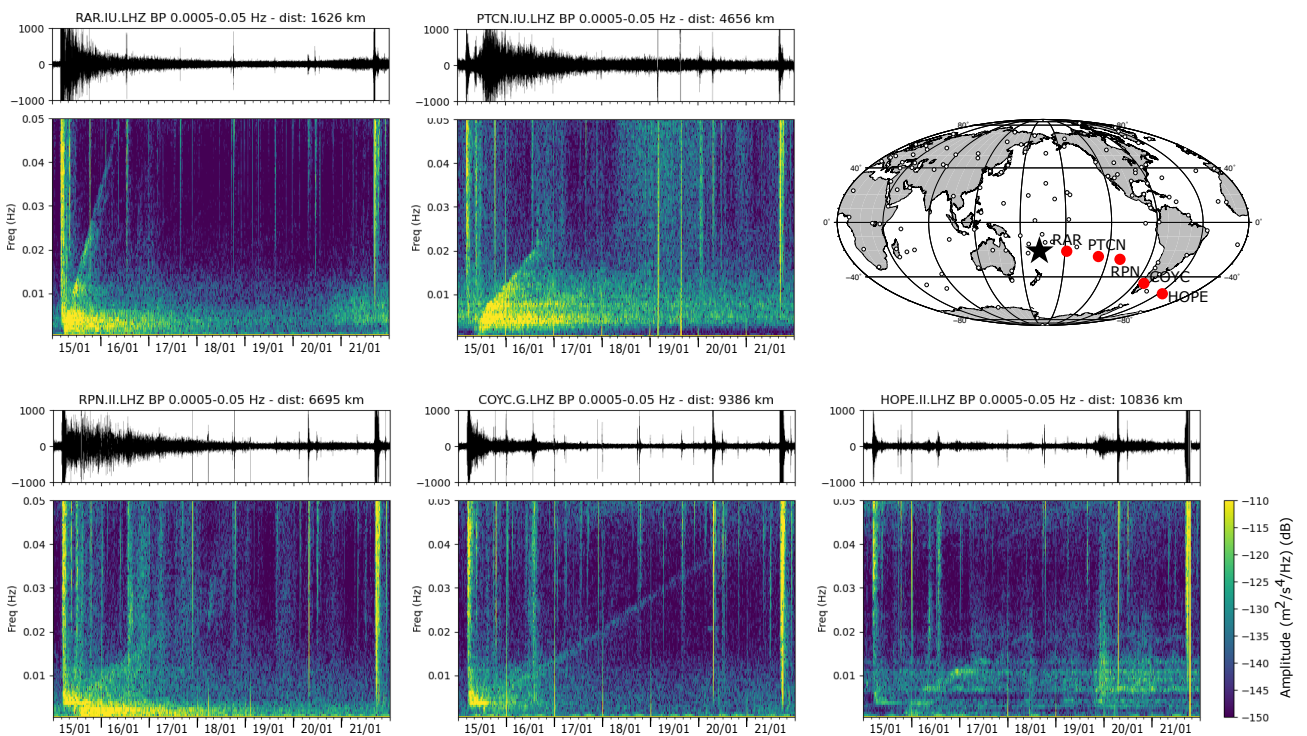


Figure 5 West-East transect across the south Pacific and Atlantic Ocean, showing gravity wave dispersion at distances ranging from 1600 to 10800 km.

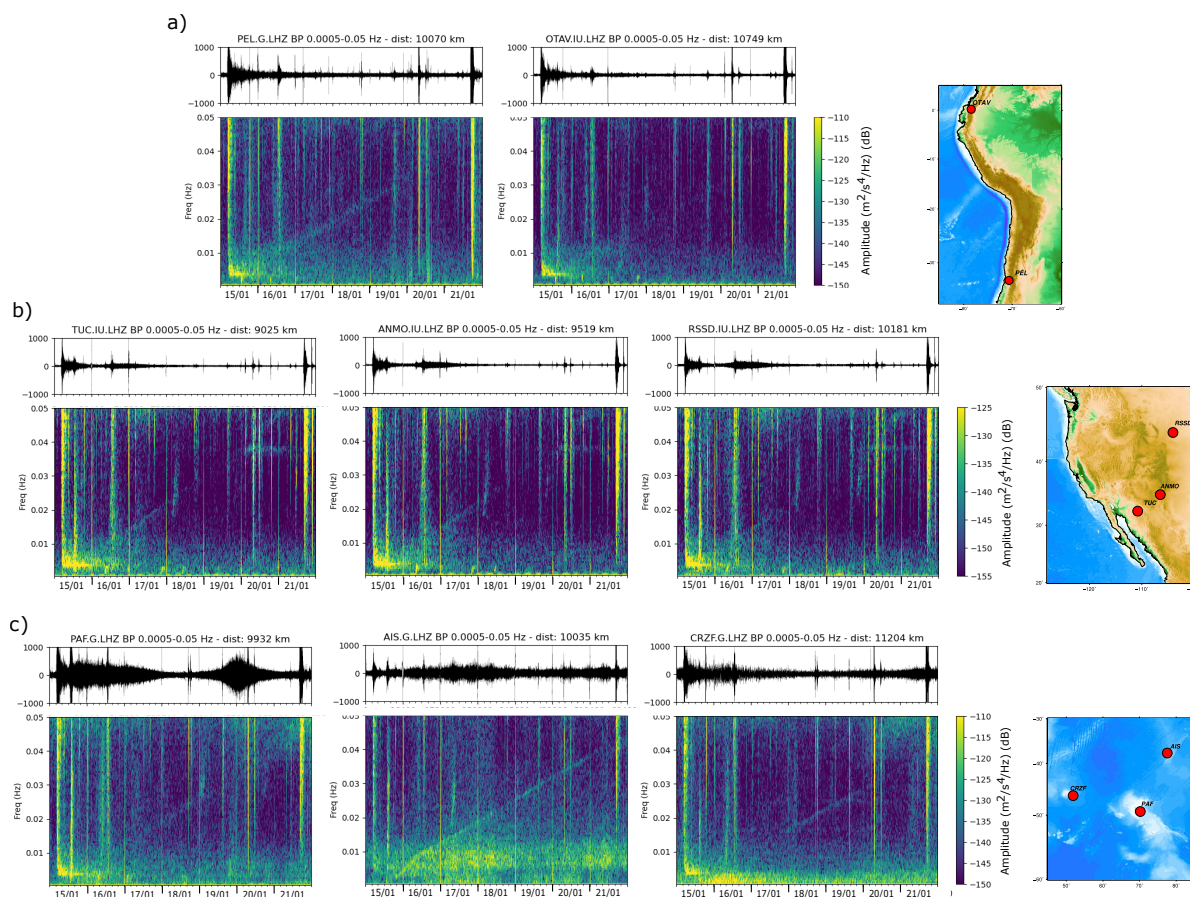


Figure 6 (a) Detection of the tsunami gravity wave at stations PEL and COYC, located in central and southern Chile. (b) Idem for stations located within the North America continent. (c) Idem for stations located in the Indian Ocean. The location of each station is shown in the inset maps

persive arrival for two to three days after the H-T eruption, consistent with the theoretical dispersion of the gravity wave generated by this eruption (Fig. 6b). Probably the most outstanding records of the tsunami-related gravity wave are obtained at the broad-band stations installed in small islands of the southern Indian Ocean, such as PAF in the Kerguelen Islands, CRZF in Ile de la Possession, and AIS in Nouvelle Amsterdam Island, at distances around 10000 km from H-T. As observed in Fig. 6c, the AIS spectrogram shows the gravity wave arrivals during more than six days, disappearing only during January 21. This is the site where the dispersive signal can be identified for the longest time.

5 Discussion and Conclusions

Previous studies based on the analysis of sea level, atmospheric, and satellite data have documented the exceptional nature of the tsunami associated with the H-T eruption. Its salient features include high propagation speed, long duration, and unexpectedly large amplitudes measured in distant coastal areas, in particular in the Pacific coasts of North and South America (Carvajal et al., 2022). The tsunami records show two different arrivals, the first one coincident with the arrival of the Lamb wave and the second one starting with the arrival

of the free tsunami wave. The arrival of the Lamb wave is marked by a clear onset in microbarographs, broadband seismic stations, and ocean-bottom pressure sensors, and coincides approximately with the onset times on the coastal tide gauges, which often show gradually increasing amplitudes over 2-4 hours. Near-surface hydroacoustic sensors in the IMS network do not detect the arrival of the precursory tsunami associated to the arrival of the Lamb wave (Le Bras et al., 2022), while deep-water pressure sensors record a clear pulse, doubling the amplitude of the atmospheric pressure signal (Matoza et al., 2022).

Omira et al. (2022) have proposed that these tsunami characteristics can be explained by a moving source generation mechanism that continuously pumps energy into the oceanic tsunami. The first water-height increase will correspond to the direct response of the ocean surface to the passage of the air-pressure disturbance, while the second arrival will correspond to the resonance between the ocean and the acoustic waves. According to their model, the interaction between acoustic and oceanic waves results in an air-water energy transfer that leads to an increase in the tsunami wave amplitude and explains the observed characteristics. The broad-band seismic records of these arrivals provide additional clues to their interpretation. As

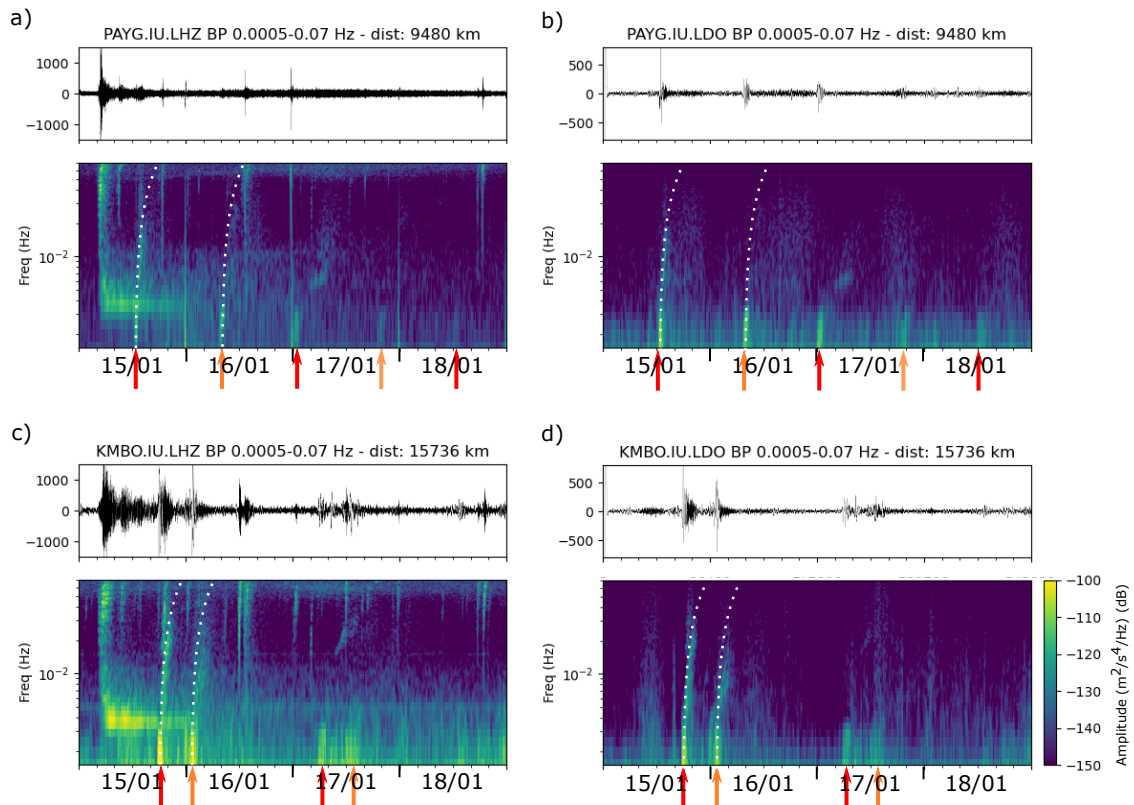


Figure 7 Seismic (a,c) and microbarometric (b,d) records at stations PAYG (a,b) and KMBO (c,d) located in the Galapagos Islands (Ecuador) and Nairobi (Kenya), respectively. Red and yellow arrows show the arrival of the successive passages of the Lamb waves following the two directions of the great arc. Dotted lines show the theoretical arrivals of a gravity wave generated at 200 km from the recording site.

shown in the previous sections, the tsunami-associated gravity wave has been seismically recorded for up to 5 days by a significant number of sites distributed within the islands and coasts of the Pacific and Indian Oceans, but also at some sites located hundreds of kilometres inland, particularly in North America. Oceanic gravity waves have been observed before using seismic instruments, mostly associated with the swell generated by distant storms. However, the global recording of long-lived dispersive waves after the H-T signal has to be considered as an exceptional feature, not observed during larger earthquake-generated tsunamis, such as the 2004 Sumatra or the 2011 Tohoku events. The most obvious difference between large earthquakes and the H-T eruption potentially affecting the tsunami generation is the highly energetic atmospheric Lamb wave generated by the H-T eruption. Therefore, it seems reasonable to relate the long duration dispersive signal observed in seismic data to a local interaction between the free oceanic tsunami and the arrival of the atmospheric pressure wave, consistently with the model presented by Omira et al. (2022). The large pressure variations detected in the ocean floor pressure sensors, but not in the shallow water hydroacoustic sensors, are also consistent with the proposed mechanism.

The inspection of seismic data at some of the stations, such as CMLA in the Azores Islands, SOK in Senegal, MBAR in Uganda, KMBO in Kenya, or PAYG in the Galapagos Islands, allows the identification of an additional dispersive signal immediately after the arrival of the Lamb wave that provides additional support for this interpretation (Fig. 7). This wave is also detected by the co-located microbarometric sensors (Fig. 7b and 7d), suggesting that it corresponds to an atmospheric perturbation. The pattern of this dispersive wave does not depend on the distance to H-T, as evidenced by the similar pattern observed at PAYG, located at a distance of 9500 km (Fig. 7a and 7b), and KMBO, at a distance of 15700 km (Fig. 7c and 7d). On the contrary, the arrival can be modeled by a local gravity wave, generated at distances of approximately 100-200 km from the recording site. This wave seems to be generated locally by the resonance effect proposed by Omira et al. (2022), hence evidencing the effects of the bidirectional interaction between the atmosphere and the oceans. It is important to note that this local wave can be identified for at least the first two passages of the Lamb wave, which once again highlights the high energy and low attenuation of this wave. However, developing a detailed physical model of the proposed interaction is needed before accepting

or discarding this tentative hypothesis.

The seismic record, of more than four days duration, of a dispersive wave in the 0.5-50 mHz band in broadband stations distributed throughout the world is an unusual feature that clearly deserves attention. The origin of this wave is related to the tsunami generated by the H-T eruption and its properties are consistent with the hypothesis of a local resonance between the free tsunami and the acoustic waves, which has been proposed to explain the unusual characteristics of the tsunami. This is further supported by the observation, in seismic and microbarometric data, of locally generated gravity waves, interpreted as a nice example of oceanic, atmospheric, and solid Earth interaction. The seismic records presented here provide a new proof of the exceptional nature of the H-T eruption and are a further confirmation that broadband seismic records can contribute, beyond their usual use in seismology, to the analysis of other sources of vibration recorded in very different zones of the seismic spectrum.

Acknowledgements

I want to acknowledge all the teams involved in the design, installation, and maintenance of broadband seismic networks around the world, which provide the essential data to carry out this type of study. I also want to thank ORFEUS EIDA (<http://www.orfeus-eu.org/data/eida/>) and FDSN (<https://www.fdsn.org/services/>) data services for providing easy access to seismic data. The manuscript has been enriched by fruitful discussions with different colleagues, and in particular with Drs. M. Ruiz and M. Schimmel. The constructive reviews of Brad Lipovsky, and an anonymous reviewer, as well as the additional comments from the editor Lise Retailleau, have clearly improved the original manuscript. This work has benefited from the infrastructure of the GEO3BCN-CSIC LabSis laboratory (<http://labsis.geo3bcn.csic.es>).

6 Data and code availability

All the seismic data used in this contribution are publicly available using the ORFEUS EIDA (<http://www.orfeus-eu.org/data/eida/>) and FDSN (<https://www.fdsn.org/services/>) data services. The seismic networks used are: IU (Albuquerque Seismological Laboratory/USGS, 2014), II (Scripps Institution of Oceanography, 1986), G (IPGP and EOST, 1982), and GE (GEOFON Data Centre, 1993).

The instrument response has been removed from the data using the standard procedures included in the Obspy package. Spectra and spectrograms have been calculated using SAC (Goldstein et al., 2003) and Obspy (Krischer et al., 2015) routines using standard parametrizations.

7 Competing interests

The author declares no competing interests.

References

- Albuquerque Seismological Laboratory/USGS. Global Seismograph Network – GSN-IRIS/USGS, 2014. doi: 10.7914/SN/IU.
- Amores, A., Monserrat, S., Marcos, M., Argüeso, D., Villalonga, J., Jordà, G., and Gomis, D. Numerical Simulation of Atmospheric Lamb Waves Generated by the 2022 Hunga-Tonga Volcanic Eruption. *Geophysical Research Letters*, 49(6), Mar. 2022. doi: 10.1029/2022gl098240.
- Astafyeva, E., Maletkii, B., Mikesell, T. D., Munaibari, E., Ravanelli, M., Coisson, P., Manta, F., and Rolland, L. The 15 January 2022 Hunga Tonga Eruption History as Inferred From Ionospheric Observations. *Geophysical Research Letters*, 49(10), May 2022. doi: 10.1029/2022gl098827.
- Aster, R. C., Lipovsky, B. P., Cole, H. M., Bromirski, P. D., Gerstoft, P., Nyblade, A., Wiens, D. A., and Stephen, R. Swell-Triggered Seismicity at the Near-Front Damage Zone of the Ross Ice Shelf. *Seismological Research Letters*, 92(5):2768–2792, Apr. 2021. doi: 10.1785/0220200478.
- Carr, J. L., Horváth, Á., Wu, D. L., and Friberg, M. D. Stereo Plume Height and Motion Retrievals for the Record-Setting Hunga Tonga-Hunga Ha'apai Eruption of 15 January 2022. *Geophysical Research Letters*, 49(9), Apr. 2022. doi: 10.1029/2022gl098131.
- Carvajal, M., Sepúlveda, I., Gubler, A., and Garreaud, R. Worldwide Signature of the 2022 Tonga Volcanic Tsunami. *Geophysical Research Letters*, 49(6), Mar. 2022. doi: 10.1029/2022gl098153.
- Cathles, L. M., Okal, E. A., and MacAyeal, D. R. Seismic observations of sea swell on the floating Ross Ice Shelf, Antarctica. *Journal of Geophysical Research: Earth Surface*, 114(F2), May 2009. doi: 10.1029/2007jf000934.
- Denamiel, C., Vasylykevych, S., Žagar, N., Zemunik, P., and Vilibić, I. Destructive Potential of Planetary Meteotsunami Waves beyond the Hunga Tonga–Hunga Ha'apai Volcano Eruption. *Bulletin of the American Meteorological Society*, 104(1):E178–E191, Jan. 2023. doi: 10.1175/bams-d-22-0164.1.
- Diaz, J. Atmosphere-solid earth coupling signals generated by the 15 January 2022 Hunga-Tonga eruption. *Communications Earth & Environment*, 3(1), Nov. 2022. doi: 10.1038/s43247-022-00616-1.
- Garza-Girón, R., Lay, T., Pollitz, F., Kanamori, H., and Rivera, L. Solid Earth–atmosphere interaction forces during the 15 January 2022 Tonga eruption. *Science Advances*, 9(2), Jan. 2023. doi: 10.1126/sciadv.add4931.
- GEOFON Data Centre. GEOFON Seismic Network, 1993. doi: 10.14470/TR560404.
- Goldstein, P., Dodge, D., Firpo, M., and Minner, L. 85.5 SAC2000: Signal processing and analysis tools for seismologists and engineers. In *International Geophysics*, pages 1613–1614. Elsevier, 2003. doi: 10.1016/s0074-6142(03)80284-x.
- Harkrider, D. and Press, F. The Krakatoa Air-Sea Waves: an Example of Pulse Propagation in Coupled Systems. *Geophysical Journal International*, 13(1-3):149–159, July 1967. doi: 10.1111/j.1365-246x.1967.tb02150.x.
- Hell, M. C., Cornelle, B. D., Gille, S. T., Miller, A. J., and Bromirski, P. D. Identifying Ocean Swell Generation Events from Ross Ice Shelf Seismic Data. *Journal of Atmospheric and Oceanic Technology*, 36(11):2171–2189, Nov. 2019. doi: 10.1175/jtech-d-19-0093.1.
- Ho, T.-C., Mori, N., and Yamada, M. Ocean gravity waves generated by the meteotsunami at the Japan Trench following the 2022 Tonga volcanic eruption. *Earth, Planets and Space*, 75(1), Feb. 2023. doi: 10.1186/s40623-023-01775-x.
- IPGP and EOST. GEOSCOPE, French global network of broad band

- seismic stations, 1982. doi: 10.18715/GEOSCOPE.G.
- Krischer, L., Megies, T., Barsch, R., Beyreuther, M., Lecocq, T., Caudron, C., and Wassermann, J. ObsPy: a bridge for seismology into the scientific Python ecosystem. *Computational Science & Discovery*, 8(1):014003, May 2015. doi: 10.1088/1749-4699/8/1/014003.
- Le Bras, R. J., Zampolli, M., Metz, D., Haralabus, G., Bittner, P., Villarroel, M., Matsumoto, H., Graham, G., and Özel, N. M. The Hunga Tonga–Hunga Ha’apai Eruption of 15 January 2022: Observations on the International Monitoring System (IMS) Hydroacoustic Stations and Synergy with Seismic and Infrasonic Sensors. *Seismological Research Letters*, 94(2A):578–588, Oct. 2022. doi: 10.1785/0220220240.
- Lipovsky, B. P. Ice Shelf Rift Propagation and the Mechanics of Wave-Induced Fracture. *Journal of Geophysical Research: Oceans*, 123(6):4014–4033, June 2018. doi: 10.1029/2017jc013664.
- Lynett, P., McCann, M., Zhou, Z., Renteria, W., Borrero, J., Greer, D., Fa’anunu, O., Bosserelle, C., Jaffe, B., Selle, S. L., Ritchie, A., Snyder, A., Nasr, B., Bott, J., Graehl, N., Synolakis, C., Ebrahimi, B., and Cinar, G. E. Diverse tsunamigenesis triggered by the Hunga Tonga–Hunga Ha’apai eruption. *Nature*, 609(7928):728–733, Aug. 2022. doi: 10.1038/s41586-022-05170-6.
- MacAyeal, D. R., Okal, E. A., Aster, R. C., Bassis, J. N., Brunt, K. M., Cathles, L. M., Drucker, R., Fricker, H. A., Kim, Y.-J., Martin, S., Okal, M. H., Sergienko, O. V., Sponsler, M. P., and Thom, J. E. Transoceanic wave propagation links iceberg calving margins of Antarctica with storms in tropics and Northern Hemisphere. *Geophysical Research Letters*, 33(17), Sept. 2006. doi: 10.1029/2006gl027235.
- Matoza, R. S., Fee, D., Assink, J. D., Iezzi, A. M., Green, D. N., Kim, K., Toney, L., Lecocq, T., Krishnamoorthy, S., Lalande, J.-M., Nishida, K., Gee, K. L., Haney, M. M., Ortiz, H. D., Brissaud, Q., Martire, L., Rolland, L., Vergados, P., Nippres, A., Park, J., Shani-Kadmiel, S., Witsil, A., Arrowsmith, S., Caudron, C., Watada, S., Perttu, A. B., Taisne, B., Mialle, P., Pichon, A. L., Vergoz, J., Hupe, P., Blom, P. S., Waxler, R., Angelis, S. D., Snively, J. B., Ringler, A. T., Anthony, R. E., Jolly, A. D., Kilgour, G., Averbuch, G., Ripepe, M., Ichihara, M., Arciniega-Ceballos, A., Astafyeva, E., Ceranna, L., Cevuard, S., Che, I.-Y., Negri, R. D., Ebeling, C. W., Evers, L. G., Franco-Marin, L. E., Gabrielson, T. B., Hafner, K., Harrison, R. G., Komjathy, A., Lacanna, G., Lyons, J., Macpherson, K. A., Marchetti, E., McKee, K. F., Mellors, R. J., Mendo-Pérez, G., Mikesell, T. D., Munaibari, E., Oyola-Merced, M., Park, I., Pilger, C., Ramos, C., Ruiz, M. C., Sabatini, R., Schwaiger, H. F., Tailpied, D., Talmadge, C., Vidot, J., Webster, J., and Wilson, D. C. Atmospheric waves and global seismoacoustic observations of the January 2022 Hunga eruption, Tonga. *Science*, 377(6601): 95–100, July 2022. doi: 10.1126/science.abo7063.
- Megies, T., Beyreuther, M., Barsch, R., Krischer, L., and Wassermann, J. ObsPy - what can it do for data centers and observatories? *Annals of Geophysics*, 54, 2011. doi: 10.4401/ag-4838.
- Munk, W. and Snodgrass, F. Measurements of southern swell at Guadalupe Island. *Deep Sea Research (1953)*, 4:272–286, Jan. 1957. doi: 10.1016/0146-6313(56)90061-2.
- National Geophysical Data Center. 2-minute Gridded Global Relief Data (ETOPO2) v2, 2006.
- Okal, E. A. Seismic Records of the 2004 Sumatra and Other Tsunamis: A Quantitative Study. In *Pageoph Topical Volumes*, pages 325–353. Birkhäuser Basel, 2007. doi: 10.1007/978-3-7643-8364-0_4.
- Omira, R., Ramalho, R. S., Kim, J., González, P. J., Kadri, U., Miranda, J. M., Carrilho, F., and Baptista, M. A. Global Tonga tsunami explained by a fast-moving atmospheric source. *Nature*, 609(7928):734–740, June 2022. doi: 10.1038/s41586-022-04926-4.
- Poplavskiy, A. S. and Le Bras, R. J. Recordings of Long-Period Fluctuations Associated with the Passage of Three Distinct Tsunamis at Broadband Seismometers Made at the International Monitoring System (IMS) Hydroacoustic T-station H06 (Socorro Island, Mexico). *Seismological Research Letters*, 84(4):567–578, July 2013. doi: 10.1785/0220120116.
- Ringler, A. T., Anthony, R. E., Aster, R. C., Taira, T., Shiro, B. R., Wilson, D. C., Angelis, S. D., Ebeling, C., Haney, M., Matoza, R. S., and Ortiz, H. D. The global seismographic network reveals atmospherically coupled normal modes excited by the 2022 Hunga Tonga eruption. *Geophysical Journal International*, 232(3):2160–2174, July 2022. doi: 10.1093/gji/ggac284.
- Scripps Institution of Oceanography. Global Seismograph Network – IRIS/IDA, 1986. doi: 10.7914/SN/II.
- Vergoz, J., Hupe, P., Listowski, C., Pichon, A. L., Garcés, M., Marchetti, E., Labazuy, P., Ceranna, L., Pilger, C., Gaebler, P., Näsholm, S., Brissaud, Q., Poli, P., Shapiro, N., Negri, R. D., and Mialle, P. IMS observations of infrasound and acoustic-gravity waves produced by the January 2022 volcanic eruption of Hunga, Tonga: A global analysis. *Earth and Planetary Science Letters*, 591:117639, Aug. 2022. doi: 10.1016/j.epsl.2022.117639.
- Wright, C. J., Hindley, N. P., Alexander, M. J., Barlow, M., Hoffmann, L., Mitchell, C. N., Prata, F., Bouillon, M., Carstens, J., Clerbaux, C., Osprey, S. M., Powell, N., Randall, C. E., and Yue, J. Surface-to-space atmospheric waves from Hunga Tonga–Hunga Ha’apai eruption. *Nature*, 609(7928):741–746, June 2022. doi: 10.1038/s41586-022-05012-5.
- Yuan, X., Kind, R., and Pedersen, H. A. Seismic monitoring of the Indian Ocean tsunami. *Geophysical Research Letters*, 32(15), Aug. 2005. doi: 10.1029/2005gl023464.
- Zhou, Y., Niu, X., Liu, H., Zhao, G., and Ye, X. Tsunami waves induced by the atmospheric pressure disturbance originating from the 2022 volcanic eruption in Tonga. *Applied Ocean Research*, 130: 103447, Jan. 2023. doi: 10.1016/j.apor.2022.103447.

The article *Seismic record of a long duration dispersive signal after the 15 January 2022 Hunga-Tonga eruption* © 2023 by J. Diaz is licensed under CC BY 4.0.